Behaviour of reinforced full scale embankment on hard ground in Phitsanulok, Thailand

S. Shrestha[1], D. T. Bergado[2], T. Hino[3]

[1] *Lecturer (Research Fellow), Institute of Lowland and Marine Research, Saga University, Japan*
[2] *Emeritus Professor, Asian Institute of Technology, Bangkok, Thailand.*
[3] *Professor, Institute of Lowland and Marine Research, Saga University, Japan*
[#] Corresponding author; < S. Shrestha; Email address: shresthasailesh@gmail.com >

Abstract—*A full-scale test embankment (6 m height) constructed by Department of Highways, the Bureau of Road Research and Development in Phitsanulok, Thailand was simulated using FEM 2D. A surcharge fill of 1.2 m thick without reinforcements was added at the top of the embankment equivalent to 2 tsm of load. One side of this embankment was reinforced with polymeric reinforcements consisting polyester (PET), polypropylene (PP) and high density polyethylene (HDPE) and referred as reinforced steep slope (RSS), which is at an angle of 70 degrees from horizontal. The other side of the embankment was reinforced with metallic reinforcements consisting of metallic strips (MS) and steel wire grids (SWG) combined with precast concrete panel and termed as mechanically stabilized earth wall (MSEW). The objective was to compare the effectiveness of different types of polymeric and metallic reinforcements in terms of the behaviour of the embankment and the reliability of the finite element method (FEM 2D) to analyse the behaviour of the embankment. The simulated results were compared with measured data. The results obtained from FEM 2D have good agreement with the field measurements in terms of vertical and lateral deformations of the embankment at the MSEW side. However, there were discrepancies between measured data and FEM 2D simulations at the RSS side due to its limitations. The FEM 2D simulation overpredicted the vertical settlements in the foundation which affected the prediction of the lateral displacements.*

Keywords—**Embankment, hard ground, FEM, metallic reinforcements.**

I. INTRODUCTION

Embankment reinforcement/MSE wall have become the widely-used method to control large differential settlement by increasing the tensile strength of the embankment soil [1,3,9,11,13,14]. Reinforcing the soil have many advantages compared with conventional reinforced concrete and concrete gravity retaining walls. Proper design of MSE wall can lead to the use of fine grained marginal soils as backfill material for reinforced soil construction, providing important cost savings and new soil reinforcement applications to reduce cost of structures that would otherwise be constructed with expensive backfill; improved performance of compacted clay structures that would otherwise be constructed without reinforcements; and use of materials, such as, nearly saturated cohesive soils and mine wastes, which would otherwise require disposal, in civil engineering construction projects.

Numerical analysis has been a strong tool for predicting the performance of the reinforced embankment / MSE wall [2-3,4-6]. Further, Chai [7] have compared the behaviour of the embankment in the soft ground, whose foundation was improved with the cement deep mixing (CDM)columns with FEM 2D and FEM 3D. The behaviour of the embankment in terms of lateral and vertical displacements was well predicted by the FEM 2D and FEM 3D. Bergado [3] suggested FEM under plane strain condition can be successively utilized to analyze the pullout and direct shear mechanisms as well as the behavior of hexagonal wire mesh reinforced embankment with silty sand backfill. Bergado and Teerawattanasuk [4] compared the reliability of FEM 2D and FEM 3D by studying two full-scale embankments; steel grid embankment having longer plan dimensions with length-to-width ratio of 3.0 (long embankment) and hexagonal wire mesh reinforced embankment having shorter plan dimensions with length-to-width ratio of 1.0 (short embankment). The actual behaviour of the steel grid reinforced long embankment corresponded more closely to the results of the FEM 2D numerical simulations. Howe ver, the actual behaviour of the hexagonal wire mesh reinforced short embankment corresponded more closely to the results of the FEM 3D numerical simulations. The geometric effects were important factors that affected the results of the numerical simulations.

This study analyses the embankment (6 m height) constructed in Phitsanulok, Thailand consisting of Reinforced Steep Slope (RSS) and Mechanically Stabilized Earth Wall (MSEW) with high strength polymeric and metallic reinforcements using FEM 2D. The simulated behaviour of this embankment were compared with the measured datas in terms of lateral and vertical displacements. Then the discussions in relation with the observed results and data are done in the lateral section. The input parameters for the soil and reinforcements, backfill materials were obtained from the laboratory testing at Asian Institute of Technology (AIT) Thailand.

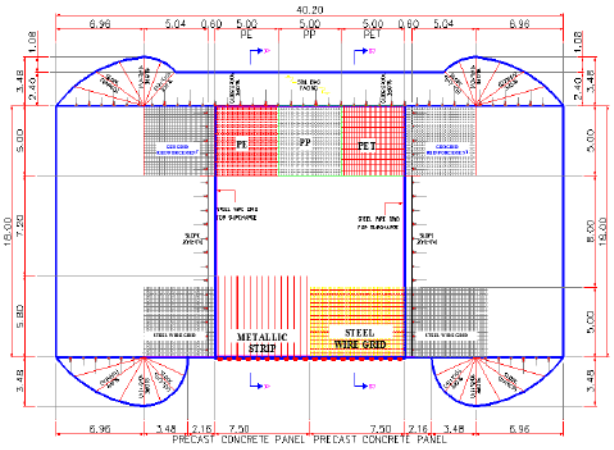

Figure 1 Plan of test MSE embankment

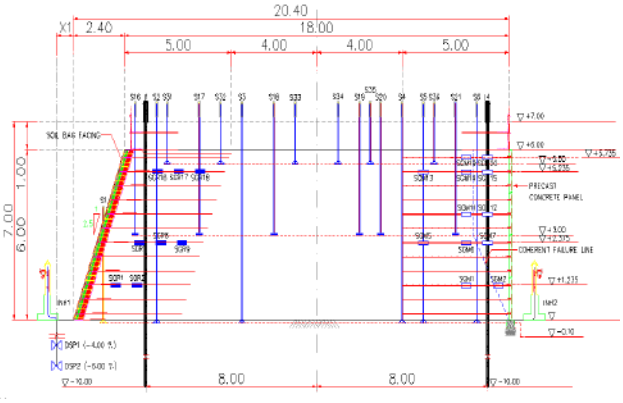

Figure 2 Cross section of MSE wall/embankment indicating the locations of monitoring instruments

II. Methodology

A. Description of the reinforced embankment

In the full scale embankment, reinforced steep slope (RSS) of 70 degrees from the horizontal with soil bags as facing was utilized in one side whereas mechanically stabilized earth wall (MSEW) with concrete panel as facing was used in another side. The test embankment with facing (RSS and MSEW) was designed up to a height of 6m. A surcharge fill 1.2 m thick was later added without reinforcement at the top of the embankment equivalent to 2 tsm load. The length of the embankment was 18 m and width was 15m. Polyester (PET), polypropylene (PP) and high density polyethylene (HDPE) geogrids were used as polymeric reinforcements in the reinforced steep slope (RSS) whereas metallic strips (MS) and steel wire grid (SWG) were utilized as metallic reinforcements in mechanically stabilized earth wall (MSEW) facing of the embankment. The vertical spacing between each reinforcement layer was 0.5 m and the length was 5 m while the upper layers of metallic strip from layer 7 to layer 12 had 5.8 m length. Different monitoring instruments were installed to monitor the vertical and lateral displacements, total stresses, excess pore water pressure, groundwater and strains in reinforcing material including inclinometers, settlement plates, total pressure cells, standpipe piezometers, vibrating wire strain gauges and fiber optic strain gauges. In addition, observation wells were installed to monitor the level of groundwater at the dummy area located more than 10 m from the embankment. The plan and cross-section views of the embankment along with the instrumentation points are shown in **Figs. 1 and 2.**

B. Modelled parameters

1) Backfill material: The material used as backfill in the embankment consisted of 50% lateritic soil mixed with 50% silty sand (by volume) and has moisture content and dry unit weight as 7% and 22.7 kN/m3, respectively. The friction angle and cohesion of this backfill material obtained from direct shear test were 42 degrees and 80 kPa. From triaxial (CU) test, the effective friction and cohesion were 37 degrees and 20 kPa, respectively. For the plane strain condition, the friction angle is converted by Lade and Lee [8] formula as ϕ' = 38.5 degrees. The various properties of backfill material are tabulated in the **Table 1.**

2) Metallic, Polymeric reinforcements and Precast concrete panel facing: The various properties of the reinforcements modelled as a geogrid material in FEM 2D are summarized in the **Table 2.** The image of the polymer and metallic reinforcements are also given in the **Fig. 3**. The comparison of the reinforcement stiffnesses from highest to lowest is as follows: metallic strip (MS), steel wire grid (SWG), polypropylene (PP), high density polyethlene (HDPE) and polyester (PET). **Table 3** gives the properties of $R_{interface}$ parameter from Large-Scale Direct Shear Test testing conducted in AIT laboratory. In this study, the precast concrete panels were modelled using plate elements. The dimensions of the panel were 1.5 m width, 1.5 m height and 0.15 m thick. The axial stiffness (EA) and the poissons ratio (v) of the panel was 42000000 kN/m and 0.15.

III. Numerical Modelling

The numerical analysis of the MSE wall/embankment was performed using FEM 2D in Plaxis 8.2 software [10]. The side boundaries were placed at a distance of two times the width of the embankment, and the bottom boundary was fixed up to the known soil layer. As shown in the **Fig. 4,** the mesh is created and the nodal points at the bottom boundary were fixed in both directions, and those on the side boundaries were fixed only in the horizontal direction. The in-situ stresses in the foundation soil were generated by the K_o procedure.

Table 1 Soil properties of the backfill soil

Property	Lateritic Soil Mixed with Sand (50:50 by Volume)
Atterberg Limit Test	LL = 20.8%, PL=17.3 %, PI=3.5%

Sieve Analysis Test	Percent Finer=0.94%, Cu=40, Cc=0.34
Unified Classification	Poorly Graded Sand (SP)
AASHTO Classification	A-2-4(0)
Compaction Test	Maximum dry unit weight (γ_d) = 22.05 kN/m^3; Optimum moisture content (OMC) = 7.0%
Direct Shear Test	Friction Angle, ϕ' =42; Cohesion,c' = 80 kPa
Triaxial (CU) Test	ϕ' =37, c' = 20 kPa
Plane strain, Triaxial (CU) Test	ϕ_{ps}'=38.5

Table 2 Material properties of reinforcements

Material Name	Tensile Strength (kN/m)	Thick-ness (mm)	Axial Stiffness, *EA* (kN/m)
Metallic Strip (MS)	277.6	4.00	88000
Steel Wire Grid (SWG)	128.1	6.00	35000
Polyester (PET)	83.6	1.50	925
Polypropylene (PP)	91.9	1.45	1360
High Density Polyethylene (HDPE)	85.8	1.91	1320

Table 3 Interface strengths from large-scale direct shear test result

Soil to	ϕ' (º)	c' (kPa)	R_{inter}
Soil	40	23	1.00
Steel Strip	36	23	0.87
Steel Grid	40	28	1.00
Polyester (PET)	33	21	0.79
Polypropylene (PP)	35	25	0.83
High Density Polyethylene (HDPE)	33	24	0.77

Then, the backfill which was divided into 13 layers, as in the field was placed on the foundation soil layer by layer. After the placement of the compacted fill layer the reinforcement was placed at interval of 0.5 m vertical spacing per stage until the completion of full height of the embankment. During this construction stage drained Mohr Coulomb analysis is used to simulate the layer by layer construction. After the completion of the full height of the embankment drained analysis is used to simulate the consolidation process for 186 days. This constitutive model was characterized by five parameters: elastic parameters (E: Young modulus, ν: Poisson's ratio) and plastic parameters (φ: friction angle, c: cohesion, and ψ: dilatancy angle). The input parameters for the numerical modelling are summarized in **Table 4.** Finally, the simulated results were compared with the measured data which are discussed in the results and discussions section.

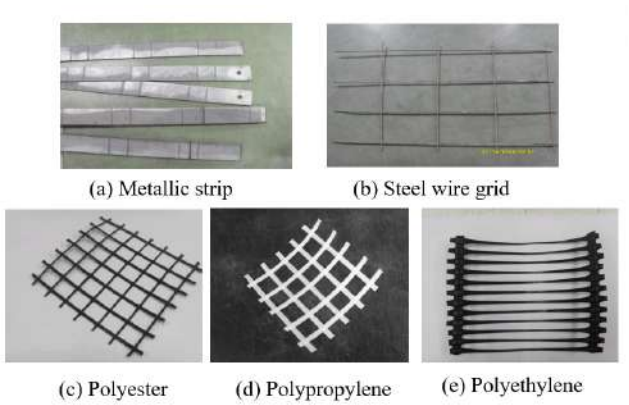

Figure 3 Metallic and Polymer reinforcements used in the test embankment

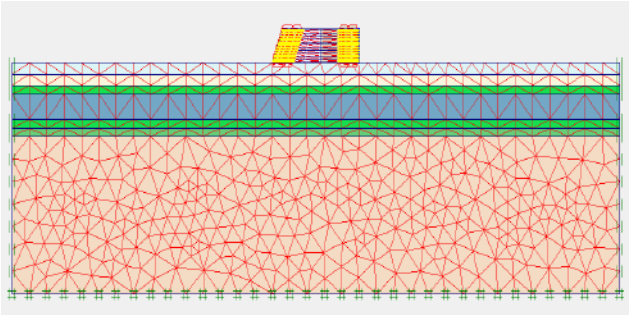

Figure 4 FEM 2D of full scale reinforced test

IV. RESULTS AND DISCUSSIONS

A. Lateral displacements

Based on the simulated results, the total lateral displacements were analysed and compared with the observed data. Inclinometers I_1, I_2, I_3, I_4 and I_5 were used to measure the lateral displacements for the PET, PP, HDPE, SWG and MS section in the field (**Fig. 2**). The lateral displacements of PET, PP and HDPE on RSS side, and SWG and MS on MSEW side obtained from field measurement by inclinometers were compared with the data from numerical simulations at 186 days after the end of the construction **(Figures 5 to 6)**. The FEM 2D (Shrestha, 2013) yielded the overall behaviour of the test embankment closer in the MSEW facing than the RSS facing. The results overpredicted below 4.50m height of the embankment on the RSS side. These discrepancies may be due to the limitations under plane strain conditions with asymmetric embankment structure. From the measured data, the lateral displacement of the RSS side with the HDPE have lowest lateral displacement at the top around 16 mm, while the side with the PETand PP (The compared data for the PP is not shown in this paper and can be referred to the Shrestha, 2013 [12])have almost same amount of lateral displacement of 27 mm. Further, for the MSEW side reinforced with metallic reinforcements and with concrete

Table 4 Material conditions and parameters used in the analysis

	Depth(m)	γt (kN/m^3)	k_x(10^{-4} m/d)	ky(10^{-4} m/d)	v	E (kPa)	c' (kPa)	φ'_{ps} (º)
Backfill material	-	22.7	-	-	12,000	10	38.5	
Dense to very dense clayey sand	0-2	19	10	5	0.35	20,000	15	30
Loose clayey sand	2-4	18	10	5	0.35	15,000	7	34
Medium dense clayey sand	4-5.5	18	10	5	0.35	25,000	5	36
Very stiff to hard silty clay	5.5-10	19	1	0.5	0.35	50,000	70	28
Dense clayey sand	11.5-13	19	10	5	0.35	30,000	8	33
Hard silty clay	13-21.45	22	1	0.5	0.35	80,000	100	26

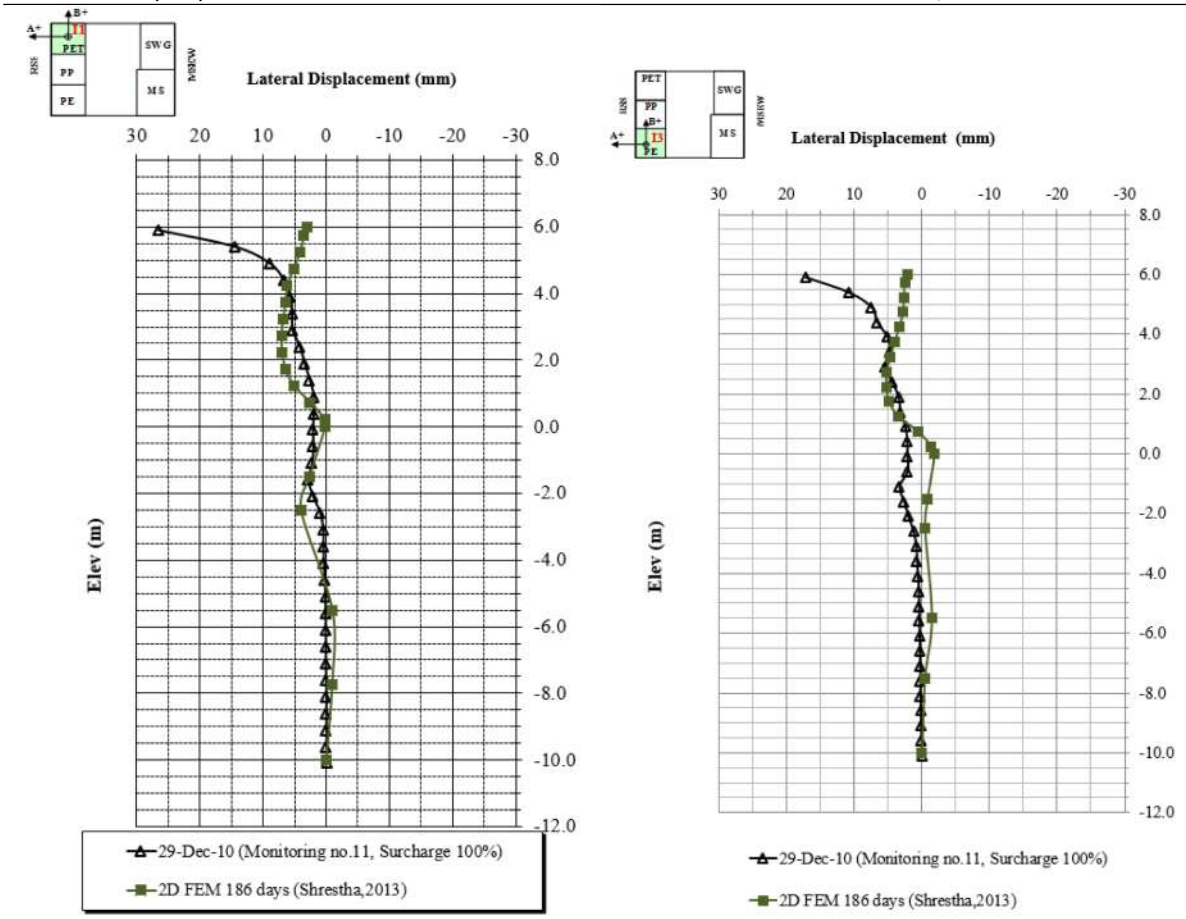

Fig. 5 Observed and simulated lateral displacements of the (a) PET and (b) HDPE

panel as facing, the lateral displacements were comparatively very smaller around 10 mm. Thus, the higher stiffness of the metallic reinforcements contributed on reducing the lateral displacements.

B. Settlements

Surface and subsurface settlement plates were installed in the embankment at different heights such as S1 to S15 at the foundation (Level 0.00 m) to measure the vertical settlements and S31 to S45 at the top (Level 5.5m) to measure the compression of the embankment (**Fig. 2**). For the PET-SWG cross-section the maximum settlement at the base of the embankment (Level 0.00m) ranged from 30 to 100 mm at 186 days after construction. The compression of the foundation was found to be slightly higher at the RSS side as shown in **Fig. 7** for this section. While, for the HDPE-MS cross-section the maximum settlement at the base of the embankment (Level 0.00m) ranged from 40 to 60 mm at 186 days after construction. The compression of the foundation was found to increase slightly towards the middle, as shown in **Fig. 8** for this section. For both cross-section FEM 2D overpredicted the vertical settlements. The over prediction may be due to the limitation of analyses under plane strain condition with asymmetric embankment structure.

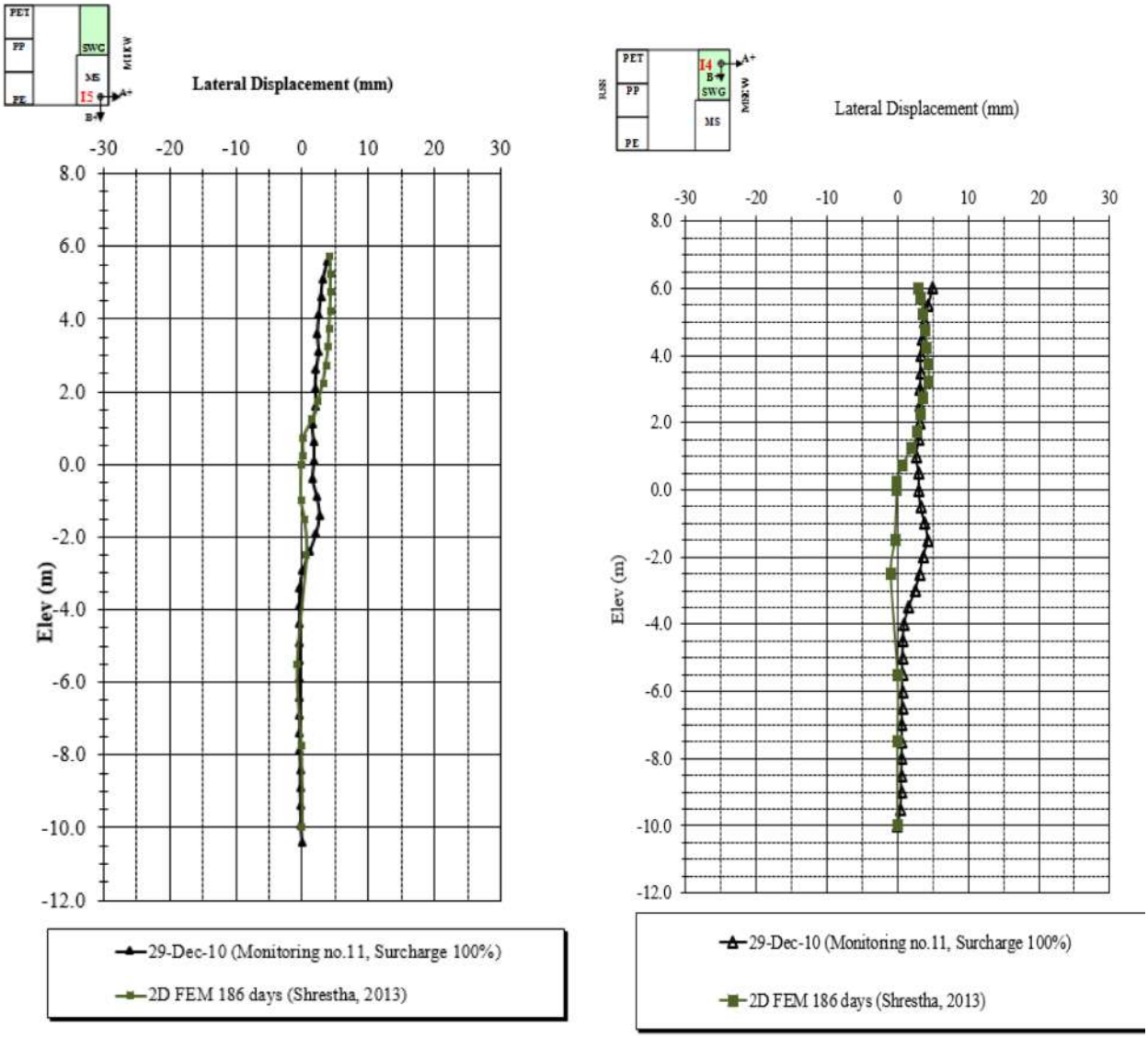

Fig. 6 Observed and simulated lateral displacements of the (a) MS and (b) SWG

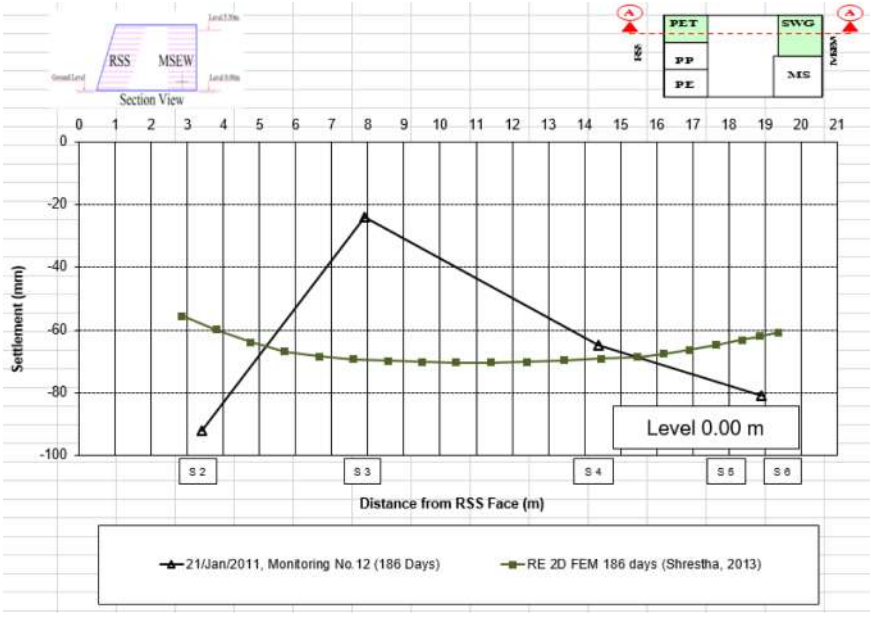

Fig. 7 Compression of the foundation at 186 days in PET-SWG cross-section

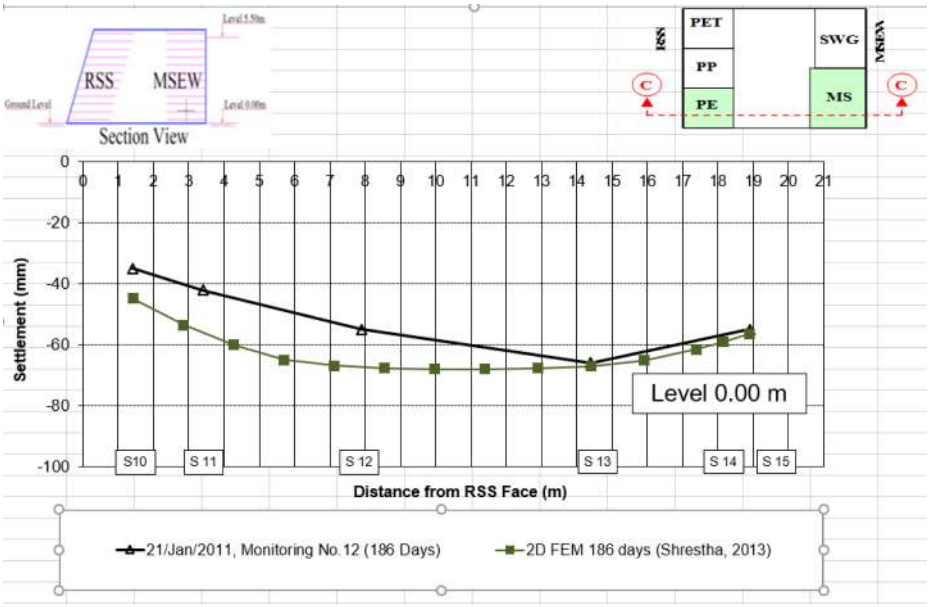

Fig. 8 Compression of the foundation at 186 days in HDPE-MS cross-section

IV. CONCLUSIONS

The full scale test embankment (6 m height) was constructed by Department of Highways in Phitsanulok, Thailand on hard foundation. The comparisons of the behaviour of both metallic and polymeric reinforcements were monitored and observed in terms of lateral and vertical displacements. The lateral displacements and vertical settlements in the MSEW faced side was less in comparison with the RSS faced side from monitored data. The RSS side has more settlement and displacement as a result of lower stiffness than MSEW side. For the polymer reinforcements, the RSS side with the HDPE have the lowest lateral and vertical displacement. For the MSEW side with the metallic reinforcements the lateral displacements were almost same for both type. The discrepancy between the measured data and the simulated data may be due to some limitations of the boundary conditions in FEM 2D for shorter embankments with asymmetric embankment structure and varying physical and engineering properties at short distances apart.

V. References

Baral P, Bergado, DT, Duangkhae S (2016) The use of polymeric and metallic geogrid on a full-scale MSE wall/embankment on hard foundation: a comparison of field data with simulation, *International Journal of Geo-Engineering*, *1*(7), 1-29.

Bergado DT, Chai JC (1995) FE analysis of grid reinforced embankment system on soft bangkok clay, *Computers and Geotechnics*,17, 447-471.

Bergado, DT, Youwai S, Teerawattanasuk C, *et al* (2003) The interaction mechanism and behavior of hexagonal wire mesh reinforce embankment with silty sand backfill on soft clay, *Computers and Geotechnics,* 30, 517-534.

Bergado DT, Teerawattanasuk C (2008) 2D and 3D numerical simuations of reinforced embankments on soft ground, *Geotextiles and Geomembranes*, 20(6), 343-365.

Chai JC, Bergado DT (1993a) Performance of reinforced embankment on Muar clay deposit, *Soils and Foundations,* 33(4), 1–17.

Chai JC, Bergado DT (1993b) Some techniques for FE analysis of embankment on soft ground, *Canadian Geotechnical Journal*, 30, 710–719.

Chai JC, Shrestha S, Hino T, *et al* (2015) 2D and 3D analyses of an embankment on clay improved by soil-cement columns, *Computers and Geotechnics*, 68, 28-37.

Lade PV, Lee KL (1976) Engineering properties of Soils. University of California, Los Angeles, CA, Report UCLA-ENG-7652.

Lai YP, Bergado DT, Lorenzo GA, *et al* (2006) Full-scale reinforced embankment on deep jet mixing improved ground. *Ground Improvement*, 10(4), 153–164.

PLAXIS 2D-Version (8.2), PLAXIS Manual, PLAXIS b.v., The Netherlands.

Shivashankar R (1991) Behavior of mechanically stabilized earth (MSE) embankment with poor quality backfills on soft clay deposits, Including a Study of the Pullout Resistances, *Doctoral Dissertation, AIT*, Bangkok, Thailand.

Shrestha S (2013) Reanalysis of full scale test embankment with polymer and metallic reinforcement on hard ground using FEM-PLAXIS 2D, *M. Eng. Thesis No. GE-13-, AIT*, Bangkok, Thailand.

Tanchaisawat T, Bergado DT, Voottipruex P (2008) Numerical simulation and sensitivity analyses of full-scale test embankment with reinforced lightweight geomaterials on soft Bangkok clay, *Geotextiles and Geomembranes*, 26, 498-511.

Voottipruex P (2000) Interaction of hexagonal wire reinforcement with silty sand backfill soil and behaviour of full scale embankment reinforced with hexagonal wire, *Doctoral Dissertation No.GE-99-1, AIT*, Bangkok, Thailand.

Response of a Floating Curved Pontoon Bridge Subjected to Tide Induced Water Surface Variation: An Analytical Approach

J Dai[1], BK Lim[2], and KK Ang[3#]

[123] *Department of Civil & Environmental Engineering, National University of Singapore, Kent Ridge, Singapore 119260*

[#] *Corresponding author; <ceeangkk@nus.edu.sg>*

Abstract— *Floating bridges are very effective solutions to linking space when the water depth is deep and/or the seabed is soft. However, they are subjected to the water surface elevation induced by the tide. This paper presents an analytical solution to the out-of-plane response of a curved floating pontoon bridge under tidal variations. Trigonometric trial functions are employed to approximate the vertical displacement and the torsional deformation of the curved bridge. The accuracy of the solution is examined through comparison against finite element analysis results. Excellent agreement is found between these results.*

Keywords— **Floating bridge, pontoon bridge, curved bridge, tidal variation**

I. INTRODUCTION

Bridges are essential in connecting islands and land parcels separated by a water body to boost economic and leisure activities. When water is very deep and/or the seabed is extremely soft at a location where a bridge is going to be built, conventional piers supporting the bridge become expensive or even impractical. Under these conditions, floating bridges may offer distinct advantages through the use of pontoons to support the bridge deck. The pontoons are supported by natural buoyancy forces and are not dependent on the sea bed condition. More importantly, if the bridge is to be relocated elsewhere when it is no longer needed, a floating bridge allows easy removal as it may be towed away by tug boats.

The use of curved layout in the floating bridge design is very effective as the environmental loads acting on the pontoons are transferred to the bridge end supports through the bridge superstructure mainly in an axial compression or tension rather than in bending and shear. A curved bridge layout also results in significantly improved resistance to the rolling motion while the water current and waves are not hindered by the existence of the structure. Examples of curved pontoon bridges include the famous Bergsøysund Bridge (see Fig. 1a) built at Bergsøyfjord near Kristiansund, Norway, in 1992 (Watanabe and Utsunomiya, 2003). It is a horizontally curved bridge spanning 845 m with a 1300 m radius of curvature. This bridge consists of a steel pipe truss superstructure resting on seven concrete pontoons. At the bridge ends, the truss work is bolted to the abutment through a flexible rod (see Fig. 1b). The flexible rod is designed to transfer the forces into the abutment mainly in axial forces. It is also designed to provide some rotational capacity to enable the absorption of the relative vertical displacement due to tidal variation.

(a)

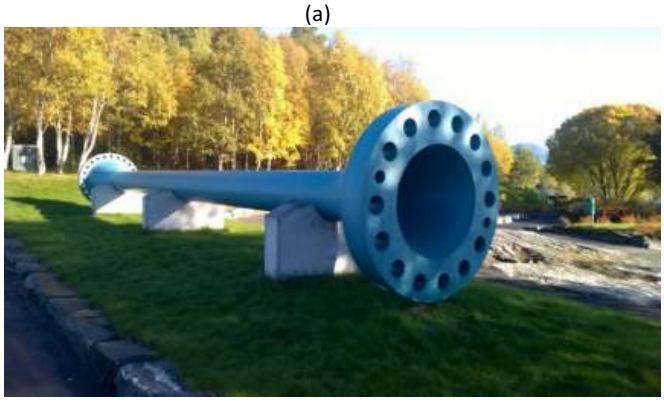

(b)

Figure 1. Bergsøysund Bridge: (a) the bridge and (b) flexible rod

Floating bridges can be very effective solutions for connecting lands separated by water. However, the tide induced sea water surface variation in some countries such as Singapore is large, about ± 2 m. Thus, it is important to examine whether a floating bridge has sufficient flexibility to adapt to the tidal variation.

The analysis of curved structures using efficient analytical approaches has interested many researchers. This includes the studies on the out-of-plane free vibration of a curved beam (Wang *et al*., 1980 and Bickford and Maganty, 1986), analysis of a one-span curved bridge subjected to moving vehicle loads (Yang *et al*., 2001), the dynamic stability of a curved rail under a moving load (Nair *et al*., 1985) and steady-state response of a continuously supported curved rail subject to a sequence of moving loads (Dai and Ang, 2015). It should be noted that the aforementioned analytical studies were confined to the case of a single-span or continuously supported

curved beam with homogeneous cross-sectional properties. For floating pontoon bridges, however, they are discretely supported by pontoons and their section may vary along its spans.

This paper presents an accurate and efficient analytical approach to the out-of-plane response of a floating curved pontoon bridge with arbitrary cross-sectional properties. Trigonometric trial functions are employed to approximate the vertical displacement and the torsional deformation of the curved bridge. The accuracy of the solution will be examined through comparison with finite element analysis results.

II. METHODOLOGY

Consider a Euler curved beam with length L, radius R, cross-sectional area $A(z)$, flexural rigidity $EI_x(z)$, and shear rigidity $GJ(z)$. The beam is simply supported at the ends. The beam torsion is also restrained at the two ends. In addition, the beam is discretely supported at the locations of the pontoons owing to the buoyancy, as shown in Figure 2. By neglecting the inertia and viscous damping terms, the out-of-plane governing equations of motion (Dai and Ang, 2015) reduce to those for a static problem that can be written as

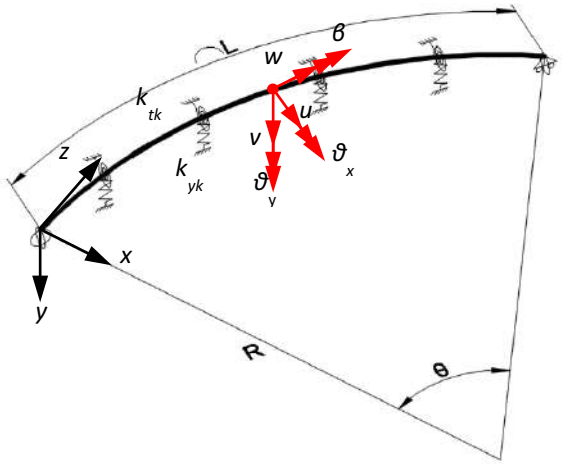

Figure 2. Coordinates and degrees of freedom of curved bridge

$$\frac{\partial^2}{\partial z^2}\left(EI_x(z)\frac{\partial^2 v}{\partial z^2}-\frac{1}{R}\beta\right)-\frac{GJ(z)}{R}\left(\frac{1}{R}\frac{\partial^2 v}{\partial z^2}+\frac{\partial^2 \beta}{\partial z^2}\right)+\sum_{k=1}^{Np}k_{yk}\left(v-H_T-H_e\right)\delta\left(z-z_k\right)=\rho A(z)g \tag{1a}$$

$$\frac{EI_x(z)}{R}\left(\frac{\beta}{R}-\frac{\partial^2 v}{\partial z^2}\right)-GJ(z)\left(\frac{\partial^2 \beta}{\partial z^2}+\frac{1}{R}\frac{\partial^2 v}{\partial z^2}\right)+\sum_{k=1}^{Np}k_{tk}\beta\delta\left(z-z_k\right)=0 \tag{1b}$$

where v and β are the vertical displacement and torsional deformation, respectively; k_{yk} and k_{tk} the vertical and torsional hydrostatic stiffness, respectively; Np refers to the number of pontoons; H_T and H_e are the tide induced surface elevation and the water surface elevation in the equilibrium state.

In view of the boundary conditions and the relationship between v and β, both vertical and torsional deformations of the curved beam can be expressed as the summation of a series of sinusoidal functions as

$$v=\sum_{i=1}^{n}q_{vi}\sin\frac{i\pi z}{L},\quad \beta=\sum_{i=1}^{n}q_{\beta i}\sin\frac{i\pi z}{L} \tag{2}$$

where q_{vi} and $q_{\beta i}$ denote the generalized coordinates of ith mode; n the number of modes. To solve the coupled differential equations, Galerkin's approach is adopted to formulate the weighted residual forms of the governing equations, which leads to ith mode governing equations

$$\sum_{j=1}^{n}a_{ij}q_{vj}+\sum_{j=1}^{n}b_{ij}q_{\beta i}=\rho g\int_0^L A(z)\sin\left(\frac{i\pi z}{L}\right)dz \tag{2a}$$

$$\sum_{j=1}^{n}c_{ij}q_{\beta j}+\sum_{j=1}^{n}d_{ij}q_{vi}=0 \tag{2b}$$

where the coefficients are

$$a_{ij}=\int_0^L\left[EI_x(z)\left(\frac{i\pi}{L}\right)^4+\frac{GJ(z)}{R^2}\left(\frac{i\pi}{L}\right)^2\right]\sin\left(\frac{i\pi z}{L}\right)\sin\left(\frac{j\pi z}{L}\right)dz+\sum_{k=1}^{Np}k_{yk}\sin\left(\frac{i\pi z_k}{L}\right)\sin\left(\frac{j\pi z_k}{L}\right) \tag{3a}$$

$$b_{ij}=\frac{1}{R}\left(\frac{i\pi}{L}\right)^2\int_0^L\left(EI_x(z)+GJ(z)\right)\sin\left(\frac{i\pi z}{L}\right)\sin\left(\frac{j\pi z}{L}\right)dz \tag{3b}$$

$$c_{ij}=\int_0^L\left[\frac{EI_x(z)}{R^2}+GJ(z)\left(\frac{i\pi}{L}\right)^2\right]\sin\left(\frac{i\pi z}{L}\right)\sin\left(\frac{j\pi z}{L}\right)dz+\sum_{k=1}^{Np}k_{tk}\sin\left(\frac{i\pi z_k}{L}\right)\sin\left(\frac{j\pi z_k}{L}\right) \tag{3c}$$

$$b_{ij}=\frac{1}{R}\left(\frac{i\pi}{L}\right)^2\int_0^L\left(EI_x(z)+GJ(z)\right)\sin\left(\frac{i\pi z}{L}\right)\sin\left(\frac{j\pi z}{L}\right)dz \tag{3d}$$

The computational effort of the coefficients depends on the variables $A(z)$, $I_x(z)$ and $J(z)$. For ease of illustration, consider Q as a line integral of a function $f(z)$ multiplied by two mode shapes over the path of the curved beam length:

$$Q=\int_0^L f(z)\sin\left(\frac{i\pi z}{L}\right)\sin\left(\frac{j\pi z}{L}\right)dz \tag{4a}$$

It is clear from Eq. (4) that $f(z)$ needs to be constant in order to fully enjoy the advantage of computational efficiency by adopting orthogonal mode shape functions. Under such a circumstance, Q is given by

$$Q=\begin{cases}\dfrac{fL}{2}, & \text{when } i=j\\ 0, & \text{when } i\neq j\end{cases} \tag{4b}$$

If $f(z)$ is symmetric with respect to the mid-span of the curved beam, partial advantage can be retained and Q is given by

$$Q=\begin{cases}\displaystyle\int_0^L f(z)\sin\left(\frac{i\pi z}{L}\right)\sin\left(\frac{j\pi z}{L}\right)\mathrm{d}z, & \text{when } |i-j| \text{ is even}\\ 0, & \text{when } |i-j| \text{ is odd}\end{cases} \tag{4c}$$

For other functions, however, such advantage is completely lost. Once the coefficients are obtained, the generalized coordinates q_{vi} and $q_{\theta i}$ can be computed by using a $2n\times 2n$ matrix manipulation.

III. RESULTS AND DISCUSSION

In this section, the accuracy of the solution presented in this paper is first examined against the results generated using a commercial finite element (FE) software. The cases of both homogeneous and inhomogeneous curved beams are considered and examined. Then, a parametric study on a homogeneous curved bridge considering different cross-sectional properties is put forward to study the effect of tidal variations on the bridge.

A. Numerical Verification of Homogeneous Curved Bridge

In order to examine the accuracy of the proposed analytical solution presented here for a floating curved pontoon bridge, a homogeneous curved beam resting over four spring supports is first considered. The properties of curved pontoon bridge are listed in Table 1. The computation of the present solution is conducted using Matlab. Figure 3a shows the convergence of the solution in terms of the maximum vertical displacement. As can be seen, the results converge fast as the number of modes involved in the computation exceeds 5. Figure 3b shows the vertical displacement of the curved pontoon bridge generated by the present solution. Also presented in this figure are the results obtained by the commercial FE software SAP2000 (Computers & Structures, 2016). Note that in the study highlighted in Fig. 3b, the bridge pontoons are not subjected to buoyancy at the initial stage. In other words, H_e in Eq. (1a) is assumed to be zero. In practical situations, however, a floating bridge is normally designed such that there is virtually zero or negligible relative vertical settlement between the pontoons and the end supports. This requires H_e of each pontoon to be evaluated. Figure 4 shows the deflection of the same curved beam but with H_e pre-calculated to ensure that the final displacements at the pontoon supports are zero. Table 2 lists the required H_e for the four pontoons. As can be seen from Figs. 3b and 4, an excellent agreement between the present approach and the FE results is found, thereby validating the accuracy of the present analytical solution.

Table 1. Curved bridge parameters

Parameter	Value	Parameter	Value
L	523.6 m	I_x	50 m^4
R	500 m	J	130 m^4
ρA	58671 kg/m	v	0.3
E	2×10^{11} N/m^2	k_{yv}	1.04×10^7 N/m

Table 2. Pontoon draft and initial buoyancy

Pontoon no.	H_e	Initial buoyancy
1	6.23 m	68112.7 kN
2	5.36 m	58660.0 kN
3	5.36 m	58660.0 kN
4	6.23 m	68112.7 kN

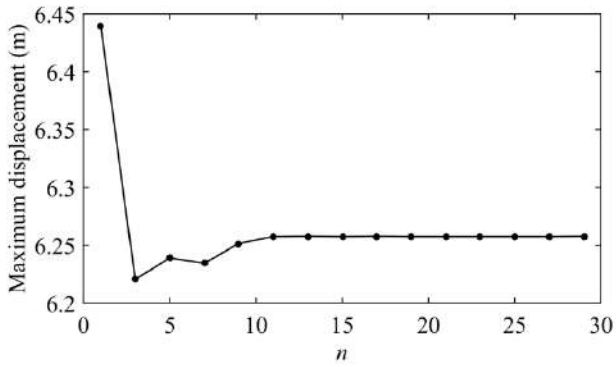

(a)

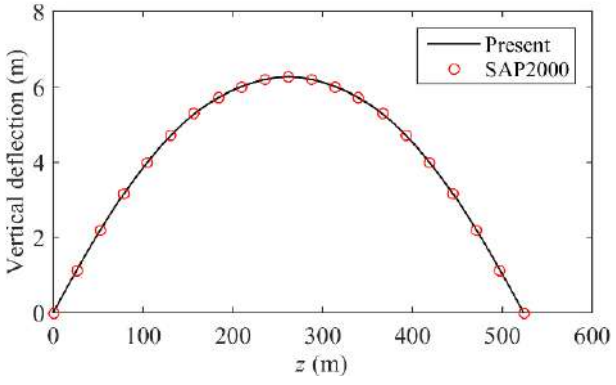

(b)

Figure 3. Numerical verification: (a) convergence and (b) vertical displacement of homogeneous curved bridge

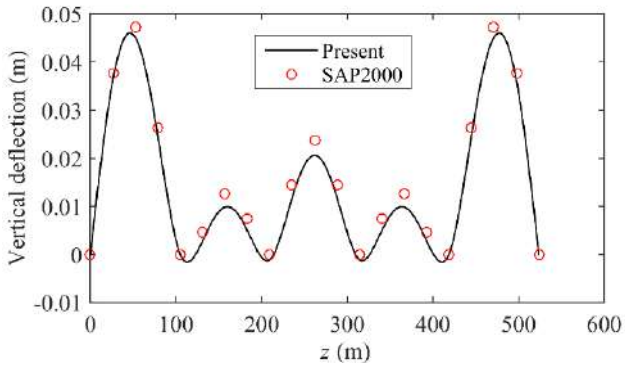

Figure 4. Vertical displacement of curved bridge

B. *Numerical Verification of Inhomogeneous Curved Bridge*

The accuracy of the proposed analytical solution for a floating curved pontoon bridge with inhomogeneous bridge section is next examined. For ease of computation and comparison against SAP2000, it is assumed here that the I_x of the bridge section remains uniform within the same span but exhibits a sudden change in different spans. Figure 5 shows the piece-wise variation of the bridge I_x throughout the entire length. Note that all the other parameters are the same as those listed in Table 1.

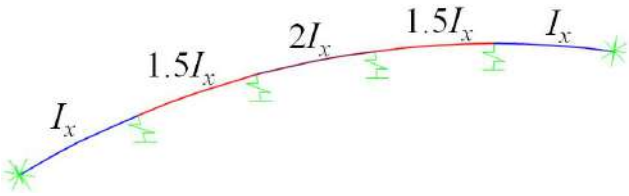

Figure 5. Inhomogeneous symmetric curved bridge

Figure 6a shows the convergence of the present solution in terms of the maximum displacement of the inhomogeneous curved bridge with respect to the number of modes included in the computation. Similar to the case of a homogeneous curved bridge, the proposed solution converges fast in view that satisfactory convergence is achieved with $n > 10$. Figure 6b presents the deflection of the curved bridge. As can be seen, the present solution matches well with the FE results.

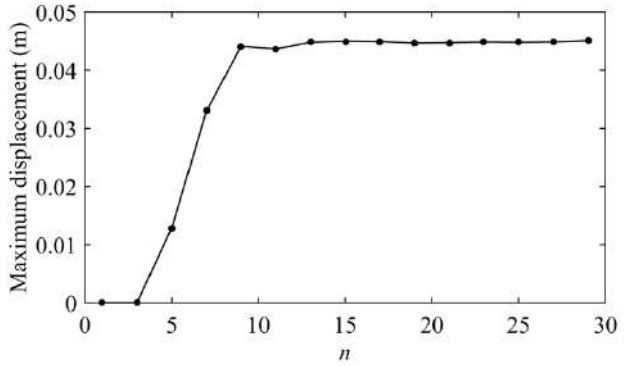

(a)

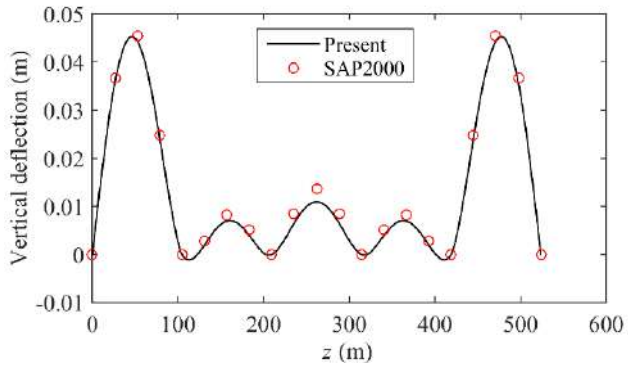

(b)

Figure 6. Numerical verification: (a) convergence and (b) vertical displacement of inhomogeneous symmetric curved bridge

The accuracy of the present solution to an inhomogeneous non-symmetric curved bridge is next examined. Figure 7 shows the piece-wise variation of the bridge superstructure I_x along its entire length. Unlike homogeneous or inhomogeneous symmetric curved bridges, the use of orthogonal mode trial functions for an inhomogeneous non-symmetric curved bridge does not lead to direct reduction in computational efforts. In other words, the evaluation of the coefficients a_{ij}, b_{ij}, c_{ij} and d_{ij} needs to be carried out according to Eq. (4a). Thus, the efficiency of the solution depends largely on the number of modes that are required in the computation.

The convergence of the analytical solution in terms of the maximum displacement of the inhomogeneous non-symmetric curved bridge with respect to the number of modes included is shown in Fig. 8a. Fortunately, the proposed solution exhibits a fast convergence rate similar to the cases of homogeneous and inhomogeneous symmetric curved bridges. Figure 8b presents the deflection of the curved bridge predicted by the present method and SAP2000. As can be seen, the present solution matches well with the FE results. The CPU time reported by Matlab for the abovementioned three cases is listed in Table 3. Clearly, accurate results for all the three cases studied can be obtained within 5 s. Note that the test is performed on a desktop PC with Intel Core i7-2600 and 16 GB memory. In view of this, it may be concluded that the developed analytical solution is able to offer accurate prediction of the curved bridge displacements efficiently.

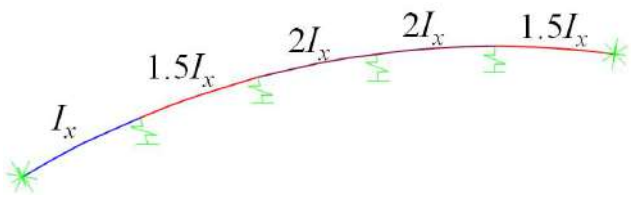

Figure 7. Inhomogeneous non-symmetric curved bridge

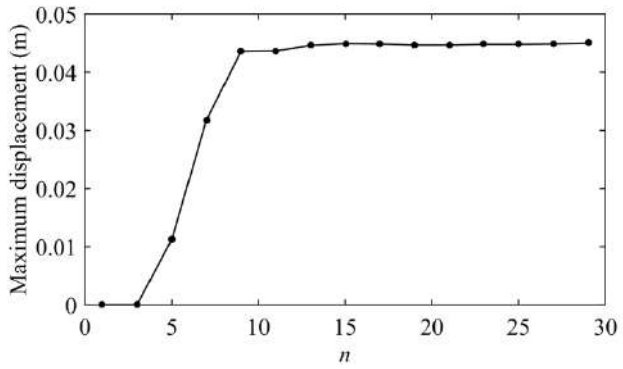

(a)

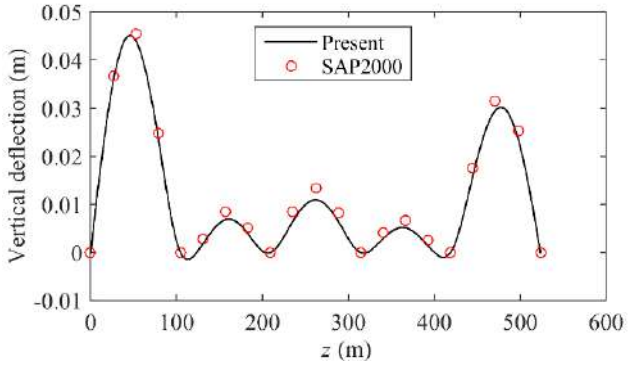

(b)

Figure 8. Numerical verification: (a) convergence and (b) vertical displacement of inhomogeneous non-symmetric curved bridge

Table 3. Computational cost

Case	No. of modes	CPU time
Homogeneous bridge	30	0.004 s
Inhomogeneous symmetric bridge	30	1.804 s
Inhomogeneous non-symmetric bridge	30	3.157 s

C. Effect of Tidal Variations on Homogeneous Curved Bridge

The effect of tide induced water surface elevation is next investigated. Figure 9 shows the vertical displacement and torsional deformation of the bridge when it is subjected to a 2 m low tide. Note that the range of the out-of-plane stiffness of the curved bridge is practically selected based on the sectional properties of the Norwegian Bergsøysund bridge. It is observed from Fig. 9 that the vertical displacement and rotation angle of the bridge start to converge when the out-of-plane second moment of inertia exceeds 10m^4. When the bridge stiffness is too low (I_x = 1m^4), the bridge spans between two adjacent pontoons exhibit noticeable deflections due to the self-weight of the bridge. Such magnitude is definitely not acceptable as it will not only hinder the serviceability of the bridge but may also lead to rupture of the superstructure and the bridge deck.

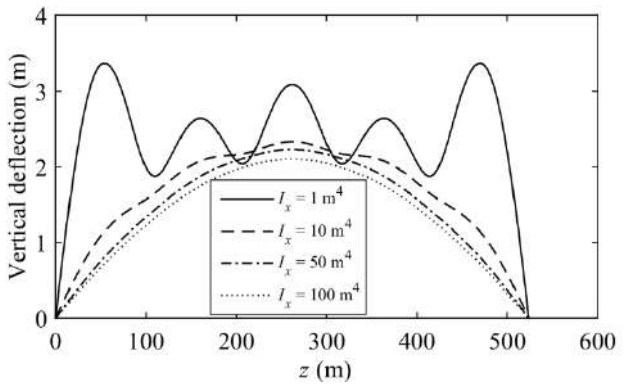

(a)

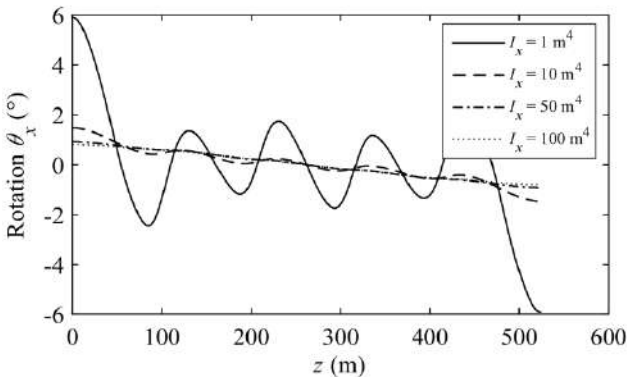

(b)

Figure 9. Homogeneous curved bridge subjected to tidal variations: (a) vertical deflection and (b) out-of-plane rotation

IV. CONCLUSION

Presented herein is an analytical approach to study the effect of tide induced sea surface elevation on a curved floating pontoon bridge. Analytical solution for the out-of-plane responses of the bridge under tidal effect was derived using trigonometric trial functions. The solution was compared with numerical results generated using the commercial finite element software SAP2000. Excellent agreement between the results was found. Furthermore, this analytical approach was shown to converge fast for both homogeneous and inhomogeneous curved bridges. Therefore, it may be concluded that the developed solution is both accurate and efficient.

On the study of the out-of-plane response of a homogeneous curved pontoon bridge under a 2 m low tide, it is found that the second moment of inertia for this particular case needs to be at least 10 m^4. For I_x in the range of 10 m^4 to 100 m^4, there appears to be no significant change in the magnitude of the bridge deformation. It is recommended that further study be carried out to investigate the resultant stresses in the curved bridge. The optimal bridge section shall fulfil both the strength and serviceability requirements and at the same time resulting in an economical design.

REFERENCES

Bickford WB, Maganty SP (1986) On the out-of-plane vibrations of thick rings, *J. Sound Vib*., 108, 503-507.

Computers & Structures (2016) *CSI Analysis Reference Manual*, Rev. 15, Berkeley, California.

Dai J, Ang KK (2015) Steady-state response of a curved beam on a viscously damped foundation subjected to a sequence of moving loads, *Proc. Inst. Mech. Eng. F J. Rail Rapid Transit*., 229, 391-442.

Nair S, Garg VK, Lai YS (1985) Dynamic stability of a curved rail under a moving load, *Appl. Math. Model*., 9, 220-224.

Wang TM, Nettleton RH, Keita B (1980) Natural frequencies for out-of-plane vibrations of continuous curved beams, *J. Sound Vib*., 68, 427-436.

Watanabe E, Utsunomiya T (2003) Analysis and design of floating bridges, *Prog. Struct. Engng. Mater*., 5, 127-144.

Yang YB, Wu CM, Yau JD (2001) Dynamic response of a horizontally curved beam subjected to vertical and horizontal moving loads, *J. Sound Vib*., 242, 519-537.

ACKNOWLEDGMENT

This material is based on research/work supported by the Singapore Ministry of National Development, National Research Foundation and JTC Corporation under L2 NIC Award No. L2NICTDF1-2015-2.